Formation of alkaline-earth template layers on Ge(100) for oxide heteroepitaxy: Self-organization of ordered islands and trenches

B. R. Lukanov,[1,2] J. W. Reiner,[1,3] F. J. Walker,[1,3] C. H. Ahn,[1,3] and E. I. Altman[1,4,*]

[1]*Center for Research on Interface Structures and Phenomena, Yale University, New Haven, Connecticut 06520, USA*

[2]*Department of Mechanical Engineering and Materials Science, Yale University, New Haven, Connecticut 06520, USA*

[3]*Department of Applied Physics, Yale University, New Haven, Connecticut 06520, USA*

[4]*Department of Chemical and Environmental Engineering, Yale University, New Haven, Connecticut 06520, USA*

(Received 29 April 2011; published 16 August 2011)

The first step required for oxide heteroepitaxy with atomically abrupt interfaces on Si and Ge(100) is the formation of an alkaline-earth template layer. The atomic structure of this template layer on Ge(100) was characterized using scanning tunneling microscopy and electron diffraction. At elevated temperatures, Sr immediately roughens the surface; a transition that can be associated with Sr displacing Ge from the surface. With increasing Sr coverage a series of ordered (3×4), (3×2), (9×1), and (6×1) phases were observed. Transitions between these phases were accompanied by morphological changes: formation of the (3×4) phase smoothed surface; transition to a local (3×2) ordering was accompanied by trench formation; ordering of the trenches led to the (9×1) structure; and finally, the (6×1) structure was characterized by atomic rows. For both Sr and Ba, highly ordered arrays of one-dimensional islands could be produced with double-height steps preventing orthogonal domain formation. We associate the morphological transitions with strain relief of the surface phases and interactions of step ledges.

DOI: 10.1103/PhysRevB.84.075330 PACS number(s): 68.35.bg, 68.37.Ef, 68.55.−a, 64.75.Yz

I. INTRODUCTION

Epitaxial crystalline oxides on semiconductors are an important class of heteroepitaxial materials in which the chemical bonding and symmetry abruptly changes across atomically sharp interfaces.[1–7] Technologically, the high dielectric constants of alkaline-earth perovskite titanates such as $SrTiO_3$ and $BaTiO_3$ have made them candidates to replace amorphous SiO_2 gate dielectrics in field-effect transistors in integrated circuits.[1,2] In addition, these and related perovskite oxides can impart new functionality to conventional microelectronic devices, including ferroelectricity, colossal magnetoresistance, and high-temperature superconductivity. Epitaxial growth of the alkaline-earth oxide-based materials relies on the formation of an alkaline-earth template layer that passivates the semiconductor surface, thus preventing the formation of an amorphous oxide at the interface.[1,2,4,5,8–10] While a number of surface phases have been observed when alkaline-earth metals are deposited onto (100) semiconductor surfaces, the atomic-scale mechanisms of the structural transformations that occur during growth, how these transformations depend on temperature, and their role in surface passivation remain unclear. Therefore, we have been using scanning tunneling microscopy (STM) in conjunction with electron diffraction, both low-energy (LEED) and reflection high-energy (RHEED), to map out the atomic-scale transformations that occur when alkaline earths are deposited onto semiconductor (100) surfaces. In this paper we will show that the alkaline earths induce long-range restructuring of Ge(100) surfaces, which is a result of surface alloy formation.

The important role of alkaline earths in promoting oxide heteroepitaxy on semiconductor (100) surfaces has led to numerous experimental and theoretical studies on the interaction of Sr and Ba with the Si(100) surface. Experiments at elevated temperatures have shown that as the alkaline-earth coverage increases, the surface evolves from the (2×1) structure exhibited by the dimerized bare Si surface to a (3×2) reconstruction at 1/6 monolayer (ML), then a (2×1) phase near 0.5 ML, which is the structure desired for oxide epitaxy, and finally a (3×1) phase near 1 ML.[4,5,9,11–27] The key question regarding these phases is whether they are simple alkaline-earth adatom structures or more complex surface alloys. Adatom models[8,28] fail to reproduce STM images of the (3×2) phase,[17,25,27] while alloy models[9,10,25] require significant Si dimer movement to occur at temperatures well below those typically required for mass transport on Si surfaces. A diffraction study on single domain vicinal Si(100) revealed a 90° rotation between the bare Si- and Sr-induced (2×1) structures at elevated temperatures that could only be explained by substantial mass transport during growth, and strongly suggesting that cooperative effects between Sr and Si reduce Si self-diffusion barriers.[9]

Alkaline-earth titanates, including ferroelectric $BaTiO_3$, have also been successfully grown on Ge(100).[2] Similar to Si, the growth process requires the formation of an alkaline-earth passivating layer. This process has not been extensively studied on Ge(100) using surface science techniques such as LEED, RHEED, and STM. Technologically, Ge is becoming an increasingly important component of high mobility channels in Si-Ge alloys and strained Ge films.[2]

In this paper, we present a comprehensive study of the effect of alkaline-earth deposition on Ge(100). Using macroscopic electron diffraction and atomic-resolution STM, it will be shown that the surface evolves from the (2×1) dimer row structure to a (3×4) reconstruction at 1/6 ML, then a (9×1) between 1/4 and 1/2 ML, and a (6×1) phase near 1 ML. As the coverage was increased past 1/6 ML, the STM images revealed the formation of trenches on the surface. For both Sr and Ba, the trenches ultimately organized into highly ordered arrays, revealing remarkable long-range order. This massive alkaline-earth-induced restructuring can be explained by surface alloying.

II. EXPERIMENT

Experiments were conducted using two ultrahigh vacuum systems: (1) a system equipped with a double-pass cylindrical mirror analyzer for Auger electron spectroscopy (AES), LEED optics, an ion gun, Ge and alkaline-earth sources, a quartz-crystal thickness monitor (QCM), and a custom-designed variable-temperature scanning tunneling microscope;[29] and (2) a custom oxide molecular beam epitaxy (MBE) chamber with *in situ* RHEED.[9] In the former chamber, alkaline earths were deposited by resistively heating a Ta coil wrapped around a quartz tube filled with Sr (or Ba) pieces, while the latter system employed commercial effusion cells. The base pressure of both ultra-high vacuum (UHV) systems was maintained in the low 10^{-10} Torr range.

For the LEED and STM measurements, the deposition rate was kept within 0.15–0.2 ML/min as measured by the QCM. For Sr, the QCM was calibrated by counting the density of Sr adatoms deposited at room temperature (where all deposited Sr remains on the surface) in STM images. Correlating the room-temperature adatom density measurements with the Sr/Ge *LMM* AES peak ratio enabled estimates of the Sr surface-atom density at high temperatures where not all of the Sr may remain on the surface. For the RHEED measurements, coverages were determined by measuring the Sr flux with a quartz-crystal microbalance that could be moved into the substrate position.

For the LEED, AES, and STM measurements, Ge(100) samples were cut from an undoped Ge(100) wafer (MTI Corp.) with a resistivity of 55.1–70.5 Ω cm. These samples were heated by conduction from resistively heated tantalum foils. The tantalum foils were pressed between the Ge samples and identical "dummy" samples by low thermal-expansion ceramic bars. *K*-type thermocouples attached to the dummy samples with a ceramic adhesive were used to measure the temperature. Entire sample assemblies were mounted on transferable molybdenum carriers.[29] Surfaces suitable for STM measurements were prepared by cycles of Ar^+ sputtering and annealing at 920 K until impurities were below the AES detection limit, followed by deposition of a 20 nm-thick Ge buffer layer at 620 K, and annealing at 920 K. This procedure produces low-defect-density surfaces with evenly spaced monatomic steps with the terrace widths governed by the misorientation of the wafer.[30] For the RHEED studies, measurements were performed using a custom-built oxide MBE chamber. As-received Ge wafers were used as substrates with the native oxide removed by desorption at high temperatures.

All STM images were recorded at room temperature. Electrochemically etched tungsten STM tips were cleaned by electron beam bombardment prior to use. The tunneling current was 0.2 nA for all STM images. Throughout the paper, sample biases are reported so that negative biases probe occupied states and positive biases probe unoccupied states.

III. RESULTS

A. Sr on Ge(100): Surface phase transitions observed with electron diffraction

Surface phase transitions as the Sr coverage was varied between 0 and 1 ML at 675 K were visualized by continuously recording RHEED patterns as Sr was deposited. Figure 1(a) shows a typical RHEED pattern recorded along the [011] zone axis after depositing 0.4 ML Sr. The image in Fig. 1(b) was constructed by stacking $[0\bar{1}1]$ horizontal cuts through each RHEED pattern in a sequence recorded during Sr deposition. Thus the image represents a time sequence with increasing coverage in the vertical direction and where each horizontal row of pixels is a cut through the pattern obtained at a given time or coverage. Starting at zero coverage from the (2 × 1) symmetry of the dimerized, clean Ge surface, the RHEED pattern evolved into a 3 × periodicity by 1/6 ML. The retention of the 1/2-order diffraction features throughout the coverage regime where the 1/3-order features were first seen suggests a (3 × 2) surface phase rather than coexistence of (2 × 1) and (3 × 1) domains. As the Sr coverage continued to increase, the spacing between the diffraction features narrowed to a distance corresponding to a 9 × reconstruction. At 0.5 ML, the surface order markedly deteriorated. Beyond 0.5 ML, the surface exhibited a 3 × periodicity that varied little as the coverage was increased towards 1 ML. Here the 1/2-order diffraction features are no longer visible and so the pattern suggests a (3 × 1) phase.

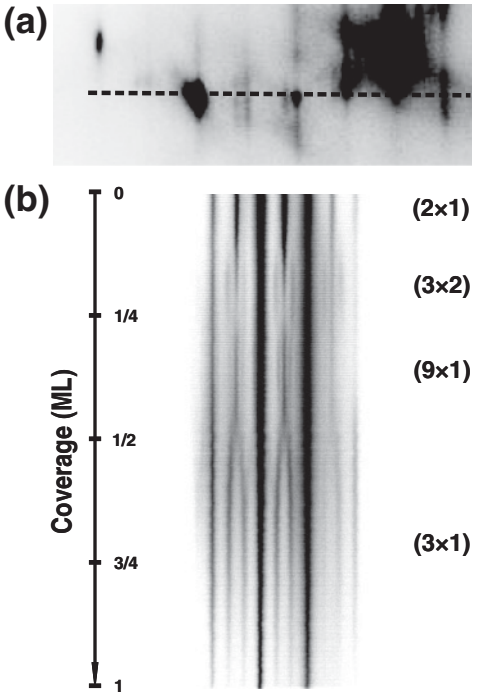

FIG. 1. (a) Typical RHEED pattern obtained during Sr deposition onto Ge(100). This pattern was obtained along the [011] azimuth after 0.4 ML Sr had been deposited. (b) RHEED time sequence constructed by stacking horizontal $[0\bar{1}1]$ cuts through a series of RHEED patterns recorded during Sr growth at 675 K. The dashed line in (a) illustrates one such cut. Time and coverage increase moving downwards. The image shows (2 × 1)→ (3 × 2) → (9 × 1) → (3 × 1) transitions as the Sr coverage was varied between 0 and 1 ML at 675 K.

The RHEED data in Fig. 1 provide valuable insight into the surface phase transitions that occur during Sr deposition on Ge(100) and were used to identify key Sr coverages for subsequent LEED and STM examination. LEED was used to obtain more complete views of the surface reciprocal lattice;

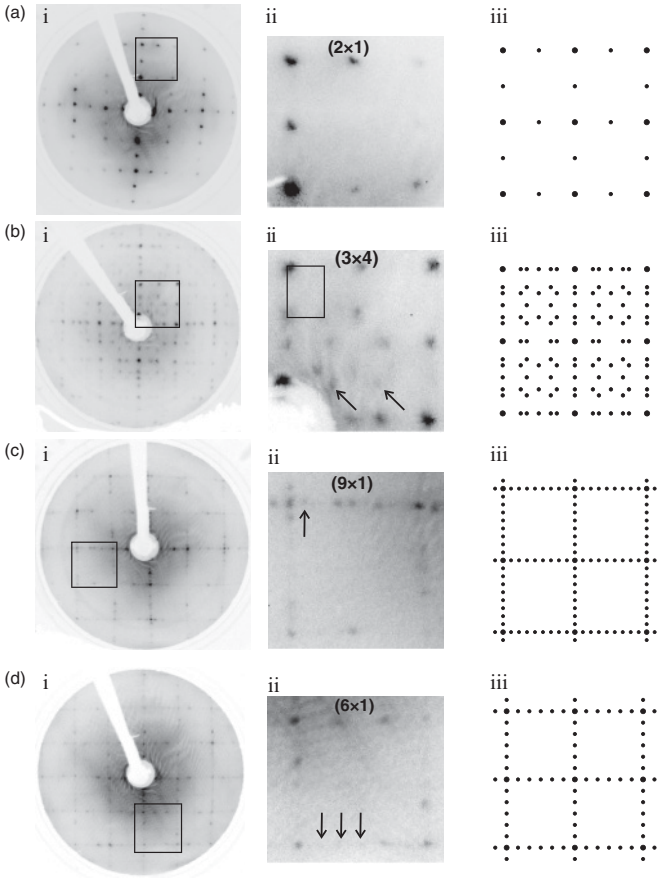

FIG. 2. LEED patterns (i), magnified insets (ii), and corresponding schematics (iii) for the Sr/Ge(100) system. (a) The (2 × 1) reconstruction of the clean Ge(100) surface, beam energy 168 eV. (b) A (3 × 4) phase at 1/6 ML Sr and 124 eV. The arrows highlight spots that distinguish the (3 × 4) structure from the (3 × 2) structure suggested by the RHEED data. (c) A (9 × 1) phase at 3/8 ML Sr and 142 eV. Arrow highlights the 1/9-order spot. (d) A (6 × 1) phase at 3/4 ML Sr and 153 eV. The arrows highlight the weak 6 × periodicity. Sr was deposited at 675 K and the surface was subsequently flashed to 900 K.

the key findings are summarized in Fig. 2. In these experiments, Sr was deposited at 675 K and the surface subsequently flashed to 900 K to obtain better order of the Sr overlayer. Consistent with the RHEED findings, weak 1/3-order symmetry was first detected with LEED after deposition of only 1/15 ML of Sr. Between 1/8 and 1/6 ML, the 1/3-order spots became very sharp, and as shown in Fig. 2(b), additional spots that could be associated with a two-domain (3 × 4) diffraction pattern were detected. At 3/8 ML, the (9 × 1) LEED pattern shown in Fig. 2(c) was obtained as anticipated from the RHEED data. As more Sr was deposited, the pattern in Fig. 2(d) emerged. At first glance, the pattern appears (3 × 1) but closer examination reveals weak 1/6-order spots suggesting a longer range (6 × 1) periodicity. The pattern in Fig. 2(d) also shows significant streaking along the [1,0] and [0,1] directions, indicative of a limited coherence length in the 6 × direction.

The additional higher-order periodicities observed in the LEED measurements can be attributed to the increased order (larger domains, fewer defects) induced by flashing the sample to high temperatures. Together, the electron diffraction data paint the following portrait of the surface phase transitions that occur during Sr deposition onto Ge at elevated temperatures: the Ge(100) (2 × 1) dimer row reconstruction is replaced by a (3 × 4) structure that saturates at 1/6 ML; above 1/6 ML a longer range (9 × 1) reconstruction develops that fades as the coverage is increased towards 1/2 ML; between 1/2 and 1 ML a (6 × 1) phase develops. This sequence of ordered phases is similar to the (2 × 1) → (3 × 2) → (1 × 2) → (3 × 1) sequence observed for Sr on Si (100),[5,9,11,12] with a couple of notable differences: the appearance of the (9 × 1) reconstruction and the lack of a well-ordered (1 × 2)-Sr phase.

B. Atomic-scale structural and morphological changes induced by alkaline earths

Scanning tunneling microscopy was used to monitor the effect of the alkaline earths on the Ge(100) surface at the atomic and nanometer scales. Figure 3 shows occupied state STM images obtained after depositing 1/15 ML of Sr at 675 K followed by flashing to 900 K. As described above, weak 1/3-order spots began to appear in LEED patterns at this coverage. The wide-range image in Fig. 3(a) shows long narrow islands elongated in orthogonal directions on adjacent terraces (examples pointed to by arrows), as well as patches that contain buckled dimer rows characteristic of the bare Ge(100) surface (circled at right), and numerous white protrusions that decorate the surface. The higher-resolution image in Fig. 3(b) allows us to identify the islands as Ge dimer rows—adjacent rows exhibit both the symmetric and the antisymmetric dimer buckling seen on bare Ge(100) surfaces.[31] Consistent with prior studies of Ge(100) homoepitaxy, the islands are elongated along the dimer row direction.[32] Compared to the clean Ge(100) surface characterized by equally spaced monatomic steps,[30] it is evident that the Sr has drastically altered the step-terrace structure of the Ge surface. The formation of elongated Ge islands can be explained by either Sr etching away the Ge terraces,[33] or Sr penetrating the surface layer and displacing Ge atoms, or dimers, which then diffuse across the surface and nucleate islands.[34] The appearance of small Ge islands on the

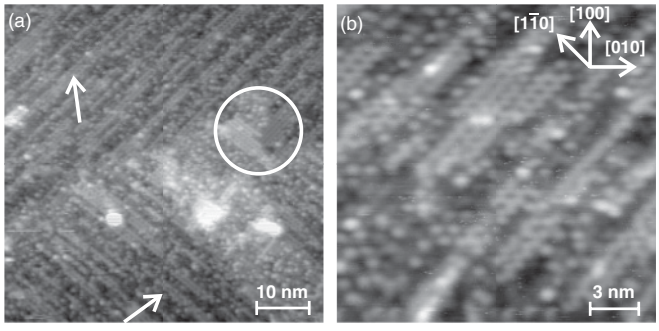

FIG. 3. Filled-state STM images of the Ge(001) surface after deposition of 1/15 ML of Sr: (a) wide-scale image and (b) high-resolution image. The arrows in (a) point to elongated islands that display the dimer row structure characteristic of Ge(100) in (b). The circle in (a) highlights a relatively unperturbed area of the Ge(100) surface. Sample biases were −1.5 V (a) and −2.25 V (b).

upper terrace towards the bottom right of Fig. 3(a) supports the latter explanation.

The white protrusions in Fig. 3 appear predominantly in the dark areas between islands but can also be seen in the midst of the dimerized islands in Fig. 3(b). Within the dimerized islands, the protrusions are found largely on top of the dimer rows but can also be seen between the dimer rows. These features are not well ordered; however, characteristic distances between them can be discerned from the images. Along the [011] and [$0\bar{1}1$] directions the protrusions are never closer than 2 × apart, while features separated by $\sqrt{2}\times$ along [010] and [001] are seen, distances that indicate that these protrusions are not responsible for the 1/3-order periodicity seen with LEED. This suggests that the dark areas between the Ge islands that could not be resolved account for the 1/3-order LEED spots. It is tempting to attribute the white protrusions in Fig. 3 to Sr adatoms; however, both theory and experiment indicate that alkaline-earth adatoms ontop of dimerized (100) surfaces appear dim in occupied state STM images, such as those in Fig. 3.[10,24] The possibility that the protrusions are Ge dimers can also be excluded. Prior studies have shown that dimers between dimer rows are difficult to detect in occupied state images, while the features in Fig. 3(b) appear similar independent of their location.[32,35] Further, studies of Ge nucleation and growth on Ge(100) indicate that Ge dimer diffusion rates are so fast that at 420 K individual Ge dimers are never seen,[32] making it highly unlikely that they could survive the 675 K Sr deposition temperature.

As the Sr coverage was increased to 1/8 ML, the morphology of the surface changed significantly. As shown in the wide-range image in Fig. 4(a), the elongated Ge dimer islands are now absent, leaving a smoother surface with peninsulas extending out from the step edges. Figures 4(b) and 4(c) reveal the structure on the peninsulas and surrounding terraces at two slightly different coverages, both near 1/8 ML. At the lower coverage [Fig. 4(b)], the surface is covered by circular bright features similar to those in Fig. 3. They are now more numerous and show some degree of order. Fourier transforms of the image in Fig. 4(b) reveal a rectangular periodicity with an aspect ratio consistent with the (3 × 4) LEED pattern obtained at this coverage. At the higher coverage [Fig. 4(c)], we again see a peninsula extending out from the step edges. The circular bright protrusions now begin to disappear and new features are revealed. Zooming in on the peninsula, the occupied state STM image in Fig. 4(d) reveals an intricate atomic-scale structure: dark undulating lines surround brighter rows of alternating short and long oblong features. The structure is clearly distinguishable from the dimerized Ge(100) surface. Measurements reveal that this is a (3 × 4) reconstruction, again consistent with the LEED pattern in Fig. 2(b). The 4 × periodicity follows the mean direction of the undulating dark lines, while the 3 × periodicity is perpendicular to them. As the bright circular features disappear while the (3 × 4) LEED pattern persists, it is apparent that this structure is responsible for the LEED pattern. We find that the structure rotates by 90° when the monatomic step from the peninsula to the adjacent terrace is descended, as expected for a diamond cubic (100) surface. In analogy to the terminology used for dimerized Si and Ge(100) surfaces,[36] straight single height steps, which parallel the dimer rows on bare Si and Ge(100) surface, will be referred to as S_A steps, while the jagged orthogonal steps will be called S_B steps as depicted in Fig. 4(c). The appearance of these (3 × 4) domains depended dramatically on the tip-sample bias; a structural model based on the bias dependence and density functional theory calculations of minimum energy structures and simulated STM images will be described in detail elsewhere.

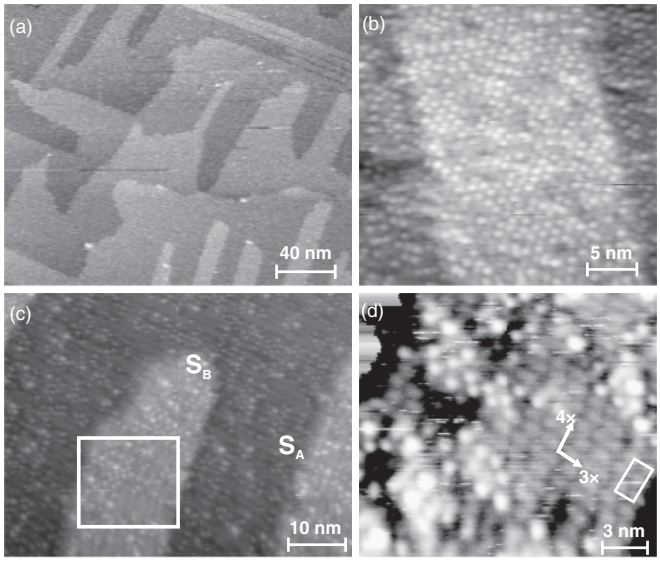

FIG. 4. STM images of 1/8 ML Sr on Ge (100) showing (a) wide-scale view of the surface; [(b) and (c)] peninsulas at two slightly different Sr coverages, stretching out onto the lower terrace; and (d) a magnified view of the peninsula in (c), with the (3 × 4) unit cell highlighted. Sample biases were −2 V (a), −2.5 V (b), and −1.25 V (c) and (d).

Slightly increasing the Sr coverage led to a more striking transformation in the Sr/Ge system. Figure 5(a) shows a filled-state, wide-scan view of the surface with five terraces, labeled T1–T5, separated by four monatomic steps. Zooming in on the terraces [Figs. 5(b) and 5(c)] reveals two phases populating the terraces in an alternating fashion—terraces T2 and T4 covered by the (3 × 4) phase discussed above and terraces T1, T3, and T5 predominantly covered by a new structure characterized by ordered arrays of bright plateaus separated by one atomic-layer-deep trenches. A closer look [Fig. 5(c)] reveals that the plateaus consist of rows of oblong features running along the length of the stripes. Measurements reveal that across each plateau the rows are three substrate unit cells apart, while parallel to the trenches the oblong features are two substrate unit cells apart, thereby giving a local (3 × 2) periodicity.

The plateau-trench structure exhibits other interesting morphological features. At the coverage in Fig. 5, the plateau widths were not uniform. Although three-row-wide plateaus predominated, plateaus containing as many as eight rows were observed. The outer rows within each plateau appear slightly brighter or raised in filled-state images. In addition, the trenches run in perpendicular directions when separated by monatomic steps and in parallel directions when separated by double-height steps as seen in Fig. 5(d). Similar to the nomenclature used for steps on Si and Ge (100) surfaces, the straight double-height step running parallel to the trenches is labeled a D_A step.[37]

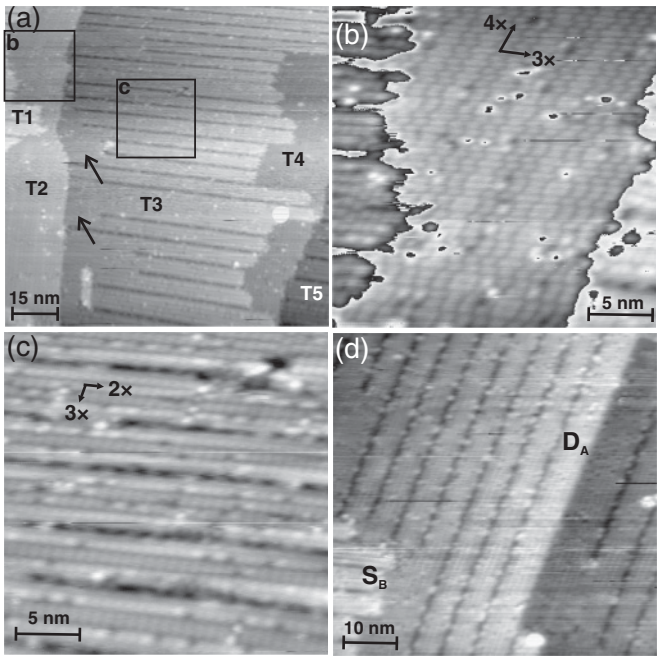

FIG. 5. STM images obtained after depositing 1/6 ML Sr on Ge(100). (a) Large-scale image showing five terraces labeled T1–T5. (b) A close-up image of the area highlighted by the box labeled "b" in (a). The image reveals the same (3 × 4) reconstruction seen in Fig. 4. (c) Magnified view of terrace T3 [area indicated by the box labeled "c" in (a)] showing parallel trenches separated by plateaus exhibiting a (3 × 2) reconstruction. (d) An area of the surface covered only by the local (3 × 2) phase showing a single and a double step. Sample biases were −2 V (a), −2.5 V (b), −2 V (c), and 3 V (d).

Interestingly, Fig. 5(b) identifies the descending steps to the right of T2 and T4 as S_A steps, while the descending steps terminating T1 and T3 can be termed S_B steps as they run perpendicular to the rows that comprise the plateaus. Similar to bare Ge and Si(100) surfaces, S_B steps are much more jagged than S_A steps. The trenches often do not continue all the way back to ascending S_A steps [see arrows in Fig. 5(a)]; when this occurs the local (3 × 2) structure gives way to the (3 × 4) structure, as illustrated in the unoccupied state image in Fig. 6. [At the imaging bias in Fig. 6, the (3 × 4) structure appears as circular bright spots at two distinct apparent heights, as will be detailed elsewhere]. This pattern indicates that the transition to the local (3 × 2) ordering and the associated trenches starts at descending S_B steps, then proceeds by replacing the (3 × 4) structure on the upper terrace. Since the local (3 × 2) order is observed after adding Sr to the (3 × 4) phase, the (3 × 2) structure must be richer in Sr. This higher Sr density coupled with the trenches means that the plateaus and trenches together form a surface phase less dense in Ge than the (3 × 4) phase. As a result, outward growth from the S_B step edges is expected as the plateau-trench phase forms. Evidence of this growth can be seen in Fig. 5(a) where T3 extends in places all the way to T5 to form a D_B step (a double-height step perpendicular to the trenches) and where T1 narrows T2 down to just a few unit cells. Consistent with this picture, it will be shown that the surface exhibits predominantly D_B steps when entirely covered by plateau-trench phases, in sharp contrast to the (3 × 4) phase, and the bare Ge(100) surface, where double-height steps are rare [Fig. 4(a)].

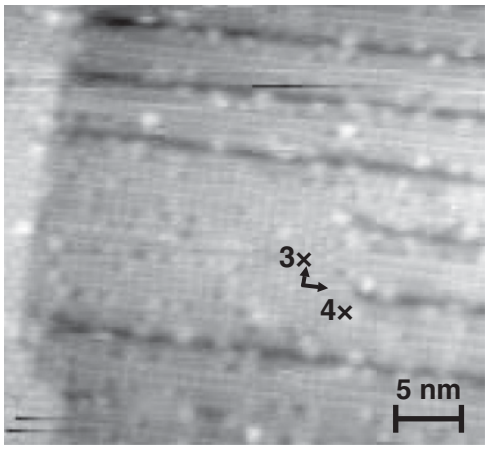

FIG. 6. An STM image obtained after depositing 1/6 ML Sr on Ge(100). The image shows that the local (3 × 2) structure (with trenches) transitions into the (3 × 4) reconstruction where the trenches end. The sample bias was 2 V.

As the Sr coverage was increased beyond 1/6 ML, the (3 × 4) structure was observed to completely disappear from the surface. As shown for 1/4 ML Sr in Fig. 7(a), the plateau-trench structure now virtually covers the entire surface. At this coverage, the atomic structure on the plateaus could no longer be resolved and the LEED pattern became diffuse. In Fig. 7(a), the distance between the trenches is not uniform; however, the predominant trench separation is between 5 and 6 nm. When the Sr coverage was increased to 3/8 ML, the coverage where the (9 × 1) LEED pattern began to emerge, the plateaus narrowed and became more ordered, as shown in Fig. 7(b). The line profile in Fig. 7(c) indicates that trenches are now 9–10 unit cells apart (3.6–4.0 nm). The source of the (9 × 1) LEED diffraction pattern is thus revealed: it is the highly ordered array of trenches on the surface that constructively interfere with the low-energy electrons. This indicates that the electron diffraction patterns are due to a longer range nano-structuring of the surface rather than the atomic arrangement of atoms on the surface. The line profile also indicates that the trenches are now deeper than one atomic layer, while the plateaus are more corrugated and disordered. Repeated attempts to obtain atomic resolution on the plateaus in this coverage range revealed only rough terraces without clear evidence of atomic order. Since the (9 × 1) electron diffraction patterns evidently reflect the plateau-trench morphology, the failure to observe any atomic structure may reflect local disorder rather than an insufficiently sharp STM tip.

Annealing surfaces with 1/4 ML of alkaline earths on Ge induced ordering of the plateau-trench structure over great distances. The image in Fig. 8(a) was obtained after depositing Sr at 675 K and then annealing at 900 K for 10 min. The image reveals two striking features: the high degree of order of the trenches and the double-height D_B steps leading to a single plateau-trench orientation. It should be noted that on larger scales monatomic steps were occasionally observed. The higher-order peaks visible in the Fourier transform of the image in Fig. 8(b) emphasize how ordered the surface is. A similar surface morphology was observed when another alkaline earth, Ba, was deposited onto Ge(100) and annealed at

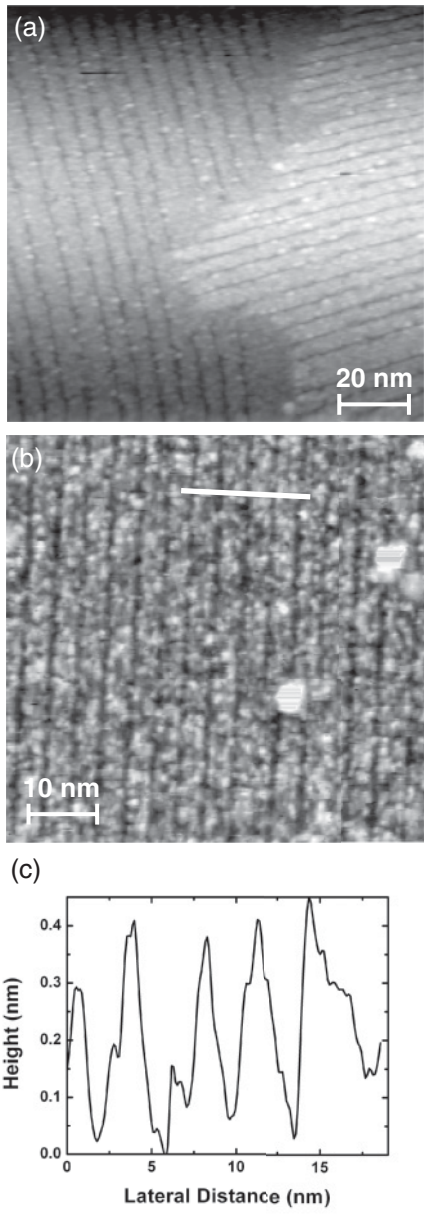

FIG. 7. STM images of Ge(100) recorded after depositing (a) 1/4 ML Sr: the entire surface is covered by an ordered array of plateaus and trenches (sample bias −2 V). (b) 3/8 ML Sr: the plateaus become narrower and more ordered (sample bias −1.75 V). Line profile (c) indicates that the average distance between trenches is between 9 and 10 unit cells (3.6–4 nm).

high temperatures, as shown in Fig. 8(c). The general features are similar to Sr with a few differences: the distances between the D_B steps are greater for Ba; the trenches are not quite as well ordered as evidenced by the appearance of only first-order peaks in the Fourier transform of the image [Fig. 8(d)]; and the trenches are further apart for Ba, 7 nm versus 4 nm for Sr. The width of strained, elongated islands has been related to strain relaxation and step energies, and so the wider islands seen for Ba implies that the Ba-induced islands may be less strained.[38] Since the exact Ba coverage is not known, however, the wider islands may indicate differences in alkaline-earth coverage rather than intrinsic differences between Sr and Ba.

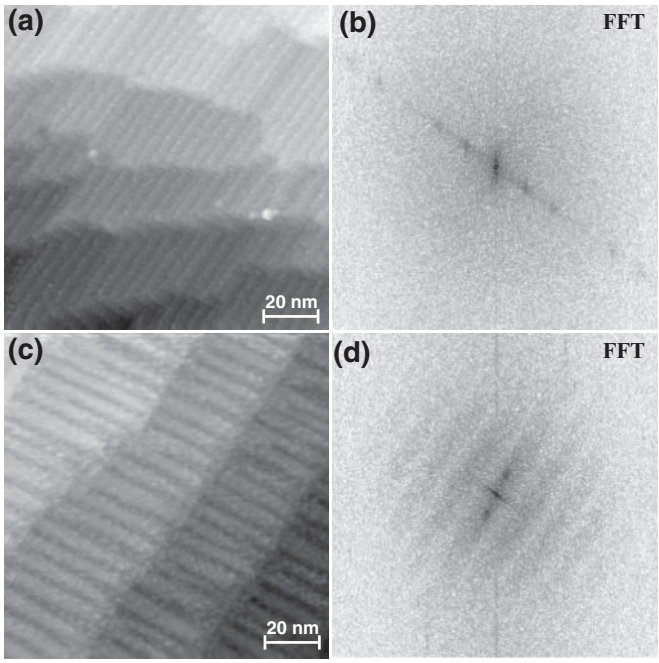

FIG. 8. STM images illustrating the effect of annealing Sr-covered Ge(100) on the surface morphology. (a) 1/4 ML Sr annealed at 900 K. (b) Fourier transform power spectrum of the image in (a) showing multiple order peaks. (c) The effect of annealing on another alkaline-earth-metal overlayer on Ge(100), Ba. (d) Fourier transform power spectrum of the STM image in (c). Sample biases were −2 V (a) and −1.5 V (b).

Still, the comparison between Sr and Ba indicates that the massive surface restructuring, the formation of long-range plateau-trench structures, and the preference for double-height steps is a general feature of alkaline-earth growth on Ge(100).

When the Sr coverage was increased to 3/4 ML where the (6 × 1) LEED pattern was recorded, a complex array of striped structures were observed, as shown in the wide-scale image in Fig. 9(a). The image shows different width and height stripes on the same terrace, 90° rotation of the stripes across monatomic steps, one- and two-atom-high islands, and narrow pits. The islands and pits are again consistent with massive restructuring of the surface rather than formation of a simple adlayer structure. Although the surface appears complex, analysis of the data reveals that the images can be explained by just two distinct building blocks, as detailed below. An ordered array of stripes can be seen at the top of Fig. 9(a); a higher-resolution image of this area is provided in Fig. 9(b). The line profile across Fig. 9(b) provided in Fig. 9(c) indicates that the spacing between the trenches in the ordered domain is 2.5 ± 0.3 nm (the uncertainty is estimated by analyzing the deviation in the spacings across multiple profiles), consistent with a 6 × periodicity. Thus these ordered domains can account for the (6 × 1) LEED pattern.

Figures 9(d) and 9(e) reveal the details of the different structures on the surface at 3/4 ML Sr. First, five terraces can be identified in Fig. 9(d). On the terrace labeled T1 at the lower right, two distinct types of stripes can be identified: broader stripes that appear similar to those seen at the lower coverage in Fig. 6, and narrower stripes that appear higher, by 0.2 ± 0.03 nm at the imaging bias of −1.75 V. The ordered terrace, T2, is

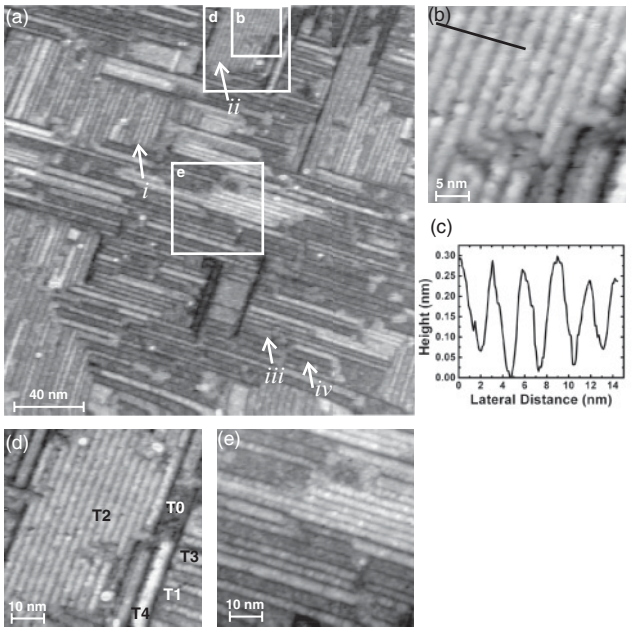

FIG. 9. Filled-state STM images of the Ge(100) surface after depositing 3/4 ML of Sr. (a) Large-scale image showing a variety of structures on the surface. Arrows *i* and *ii* point to stripes of the same width but different spacings, while arrows *iii* and *iv* point to stripes of the same height but different width. (b) Close-up view of the area highlighted by the box labeled "b" in (a). (c) Height profile taken along the line indicated in (b). (d) Magnified view of the area labeled "d" in (a). (e) Close-up view of the area in the middle of image (a) highlighted by the box labeled "e." Sample biases were −2 V in (a), (d), and (e) and −1.75 V in (b).

made up solely of the latter. The bright broad strip labeled T4 is attributed to a single broad stripe two atomic steps higher than T2; a similar bright broad stripe to the right, labeled T3, is assigned to a single stripe two atomic steps higher than T1. Analysis of the image in Fig. 9(e) reinforces this picture. Here all the stripes are oriented in the same direction and the height differences between stripes of the same type on the upper and lower levels are consistent with double-height steps. The image shows that the narrower, higher stripes are always the same width, but their spacing varies. Some of these narrower stripes also show evidence of atomic-scale circular features. Now referring back to Fig. 9(a), we see that the complexity of the surface morphology arises from (1) two different types of stripes that differ in height, width, and corrugation; (2) two-atom-high islands as narrow as a single stripe; (3) variation in the spacing of the narrow stripes as pointed to by arrows (i) and (ii); and (4) variation in the width of the wider stripes as pointed to by arrows (iii) and (iv) (and also seen in Figs. 5 and 7). Consistent with the electron diffraction data that indicated that the (6 × 1) structure covers the surface at 1 ML Sr, it is not surprising that at 3/4 ML Sr, the wider stripes featured at the lower coverage coexist with the narrower stripes that organize into 6 × domains.

IV. DISCUSSION

The results reveal the following structural and morphological transitions when increasing amounts of Sr are added to Ge(100) surfaces at elevated temperatures: (1) an apparent etching away of the Ge terraces accompanied by the appearance of raised spherical features on the surface; (2) the formation of a (3 × 4) structure accompanied by a smoothing of the surface and the formation of large peninsulas; (3) the formation of long straight trenches on the surface accompanied by a transition from a (3 × 4) to local (3 × 2) structure on the plateaus between the trenches; (4) ordering of the trenches into a 9 × periodicity with a preference for double-height steps creating large domains where the trenches are all oriented in the same direction; and (5) transition to a second type of stripe or plateau on the surface with a characteristic 6 × spacing between stripes. Electron diffraction data for Ba growth on Ge(100) along with the STM data in Fig. 8 suggest that the sequence outlined above for Sr applies more generally to alkaline earths on Ge(100).

There are several interesting aspects to this growth sequence. First, it is obvious that the massive surface restructuring cannot be explained by simple adatom structures, rather the morphological changes suggest alkaline earths penetrate the surface to form surface alloys. The surface alloys are less rich in Ge than the original surface and so alloy formation is accompanied by Ge ejection onto the terraces. At the lowest alkaline-earth coverages (Fig. 3), the ejected Ge atoms or dimers collide with one another nucleating new Ge(100) terraces with the characteristic buckled dimer reconstructions. As the alkaline-earth coverage increases, the added layers created by Ge ejection take on the same structure as the underlying terraces, (4 × 3) for Sr. Increasing the alkaline-earth coverage beyond this point leads to the second striking feature, the formation of straight, highly ordered arrays of trenches.

As described in the Introduction, there has been a debate in the literature over whether Sr-induced reconstructions on Si(100) are due to Sr adatoms or more complex alloy phases. One argument used to bolster the case for adatom structures has been that the temperatures are too low to either break Si dimers or induce significant Si dimer motion on the surface. Although less energy is required to break Ge dimers or induce self-diffusion of Ge dimers, the growth temperatures employed in this study are also significantly lower (675 K versus a typical growth temperature of 875 K for Si) and well below those required to break Ge dimers or restructure Ge surfaces.[39] It should be noted that LEED indicated that the brief flashing to higher temperatures did not induce new structures but simply increased the surface order. The low temperatures, however, do not preclude surface alloy formation, only that alloy formation does not occur through a sequential process initiated by either Ge dimer breaking or ejection onto the terraces. It has been shown that Au induces massive surface restructuring of Ge(100) consistent with Au penetration into the surface at temperatures as low as 475 K.[40] Recent studies have indicated that the interaction of Au with Ge(100) at these modest temperatures induces changes in the Ge surface that include the four outermost layers.[41] In this case, the low-temperature surface restructuring was associated with a concerted low-energy pathway involving both Au and Ge in the transition state.[40] Thus the relatively low temperatures at which the alkaline earths cause massive surface restructuring point towards a similar concerted mechanism. Such concerted exchange and diffusion mechanisms are now well established

for metal surfaces where they similarly explain diffusion and surface alloying at unexpectedly low temperatures.[42,43] Theory has also demonstrated that concerted exchange mechanisms can dramatically lower the barrier to break Si dimers when Sr is present on the surface.[10] These findings indicate that caution should be exercised in predicting the behavior of multicomponent surfaces based on the dynamics and energetics of the constituent pure surfaces.

The formation of trenches on the surface can be associated with strain relief. The inclusion of larger Sr atoms (0.192 nm covalent radius compared to 0.122 nm for Ge) in a surface constrained to match the underlying bulk Ge leads to compressive strain; the trenches provide space for the surface layer to expand and relieve this strain. The tetrahedral bonding in the diamond cubic structure leads to dimer row reconstructions of (100) surfaces and uniaxial strain on (100) terraces. As a result, growth on, and etching of, these surfaces typically leads to elongated islands and pits,[32,33,36,44] accounting for the alkaline-earth-induced formation of trenches and elongated plateaus rather than square islands.[36] The trench edges can be viewed as essentially step edges. In this regard it is not surprising that the trenches are extremely straight since the trench edges parallel dimer-row-like features on the plateaus [see Fig. 5(d)], and kink energies are high in this direction.[36]

More interestingly, the islands and trenches self-organize over an unusually long range, with a narrow distribution of island sizes. Peaked distributions of island sizes for strained systems have been explained in terms of thermodynamics. It has been shown that the relaxation energy of strained islands can lead to a minimum in the energy per atom in the island and thus a favored island size.[38,45] Following the work of Tersoff and Tromp,[38] the energy per atom, or reduced energy $\tilde{E}(n) = E(n)/n$, of noninteracting one-dimensional islands can be expressed as

$$\tilde{E}(n) = E_b + a_s n^{-1} - a_r n^{-1} \ln(n), \qquad (1)$$

where the first term is the binding energy per atom and the last two terms describe the surface and relaxation energies, respectively. Both a_s and a_r are positive constants: a_s is a function of the island and substrate surface energies and the island-substrate interfacial energy, while a_r is a function of the Poisson ratio and shear modulus of the substrate.[43] While this equation passes through a minimum, at nonzero temperatures the entropy of mixing of different sized islands will lead to a distribution of island sizes, generally assumed to take on a Gibbs-Boltzmann distribution of the form [45]

$$P_n = \exp\left(\frac{n[\mu - \tilde{E}(n)]}{kT}\right), \qquad (2)$$

where P_n is the probability of an n-sized island and μ is its chemical potential. A narrow distribution will occur if the chemical potential approaches the reduced energy, a situation that occurs when Eq. (1) has a sharp minimum, which is the case when a_r is large. This suggests that the well-ordered trench-plateau structure is the result of an unusually large and anisotropic relaxation energy, the anisotropy undoubtedly arising from the asymmetry of the (3 × 2) structure. While Eqs. (1) and (2) were derived for distant, noninteracting islands, island-island interactions generally broaden island size distributions,[45] though scenarios have been identified where island-island interactions can improve self-organization.[46]

It has been shown that growth kinetics can also lead to self-organization of strained islands as a stable state. Simulations of island formation during heteroepitaxial growth have shown that systems with sufficiently large lattice mismatch naturally evolve into a state with a narrow island size distribution.[47] The self-organization mechanism involves a lowering of the energy barrier for diffusion due to surface strain, and implies that for large islands, the strain energy at the islands' edges becomes comparable to the binding energy of the edge atoms. This causes a gradual dissolution of large islands, smaller average island sizes, and a narrower island size distribution; i.e., the reverse of Ostwald ripening.

V. SUMMARY

The deposition of Sr on Ge(100) at elevated temperatures was characterized on a macroscopic scale using RHEED and LEED and on the atomic scale using STM. The results revealed a series of phase transitions as the Sr coverage was increased: a (4 × 3) phase initially, followed by a local (3 × 2) ordering, then a (9 × 1) structure, and finally a (6 × 1) periodicity. Each phase transition was accompanied by substantial changes in the surface morphology. The observed massive restructuring could not be explained in terms of a simple Sr adlayer, but rather provided evidence for Sr-Ge surface alloy formation. Lattice mismatch strain between alkaline-earth-Ge surface alloys and the underlying Ge can account for the striking long-range ordering of trenches observed for roughly 1/4 ML Sr and Ba.

ACKNOWLEDGMENTS

The authors would like to thank Sohrab Ismail-Beigi, Kevin Garrity, Todd Schwendemann, Harry Mönig, Matthew Herdiech, and Min Li for their help in carrying out this work. This project was supported by the National Science Foundation through the Yale Materials Research Science and Engineering Center (Grant No. MRSEC DMR-0520495) and through Grant No. DMR-1006265.

*Corresponding author: Department of Chemical and Environmental Engineering, Yale University, P.O. Box 208260, New Haven, CT 06511; eric.altman@yale.edu

[1] R. A. McKee, F. J. Walker, and M. F. Chisholm, Phys. Rev. Lett. **81**, 3014 (1998).

[2] R. A. McKee, F. J. Walker, and M. F. Chisholm, Science **293**, 468 (2001).

[3] H. Mori and H. Ishiwara, Jpn. J. Appl. Phys., Part 2 **30**, L1415 (1991).

[4] Y. Liang, S. Gan, and M. Engelhard, Appl. Phys. Lett. **79**, 3591 (2001).

[5] J. Lettieri, J. H. Haeni, and D. G. Schlom, J. Vac. Sci. Technol. A **20**, 1332 (2002).

[6] C. J. Först, C. R. Ashman, K. Schwarz, and P. E. Blöchl, Nature (London) **427**, 53 (2004).

[7] X. Zhang, A. A. Demkov, H. Li, X. Hu, Y. Wei, and J. Kulik, Phys. Rev. B **68**, 125323 (2003).

[8]C. R. Ashman, C. J. Först, K. Schwarz, and P. E. Blöchl, Phys. Rev. B **69**, 075309 (2004).
[9]J. W. Reiner, K. F. Garrity, F. J. Walker, S. Ismail-Beigi, and C. H. Ahn, Phys. Rev. Lett. **101**, 105503 (2008).
[10]K. F. Garrity and S. Ismail-Beigi, Phys. Rev. B **80**, 085306 (2009).
[11]W. C. Fan, N. J. Wu, and A. Ignatiev, Phys. Rev. B **42**, 1254 (1990).
[12]R. Z. Bakhtizin, J. Kishimoto, T. Haashizume, and T. Sakurai, J. Vac. Sci. Technol. B **14**, 1000 (1996).
[13]R. Z. Bakhtizin, J. Kishimoto, T. Haashizume, and T. Sakurai, Appl. Surf. Sci. **94-95**, 478 (1996).
[14]X. Hu, Z. Yu, J. A. Curless, R. Droopad, K. Eisenbeiser, J. L. Edwards Jr., W. J. Ooms, and D. Sarid, Appl. Surf. Sci. **181**, 103 (2001).
[15]R. A. McKee, F. J. Walker, J. R. Conner, and R. Raj, Appl. Phys. Lett. **63**, 2818 (1993).
[16]D. P. Norton, C. Park, Y. E. Lee, and J. D. Budai, J. Vac. Sci. Technol. B **20**, 257 (2002).
[17]W. Du, B. Wang, L. Xu, Z. Hu, X. Cui, B. C. Pan, J. Yang, and J. G. Hou, J. Chem. Phys. **129**, 164707 (2008).
[18]W. C. Fan and A. Ignatiev, Surf. Sci. **253**, 297 (1991).
[19]X. Hu, C. A. Peterson, D. Sarid, Z. Yu, J. Wang, D. S. Marshall, R. Droopad, J. A. Hallmark, and W. J. Ooms, Surf. Sci. **426**, 69 (1999).
[20]T. Urano, K. Tamiya, K. Ojima, S. Hongo, and T. Kanaji, Surf. Sci. **357-358**, 459 (1996).
[21]Y. Takeda, T. Urano, T. Ohtani, K. Tamiya, and S. Hongo, Surf. Sci. **402–404**, 692 (1998).
[22]D. Vlachos, M. Kamaratos, and C. Papageorgopoulos, Solid State Commun. **90**, 175 (1994).
[23]R. A. McKee, F. J. Walker, J. R. Conner, E. D. Specht, and D. E. Zelmon, Appl. Phys. Lett. **59**, 782 (1991)
[24]X. Yao, X. Hu, D. Sarid, Z. Yu, J. Wang, D. S. Marshall, R. Droopad, J. K. Abrokwah, J. A. Hallmark, and W. J. Ooms, Phys. Rev. B **59**, 5115 (1999).
[25]X. Hu, X. Yao, C. A. Peterson, D. Sarid, Z. Yu, J. Wang, D. S. Marshall, R. Droopad, J. A. Hallmark, and W. J. Ooms, Surf. Sci. **445**, 256 (2000).
[26]K. Ojima, M. Yoshimura, and K. Ueda, Phys. Rev. B **65**, 075408 (2002).
[27]K. Ojima, M. Yoshimura, and K. Ueda, Surf. Sci. **491**, 169 (2001).
[28]A. A. Demkov and X. Zhang, J. Appl. Phys. **103**, 103710 (2008).
[29]C. Y. Nakakura, V. M. Phanse, G. Zheng, G. Bannon, E. I. Altman, and K. P. Lee, Rev. Sci. Instrum. **69**, 3215 (1998).
[30]L. H. Chan and E. I. Altman, J. Vac. Sci. Technol. A **19**, 976 (2001).
[31]H. J. W. Zandvliet, B. S. Swartzentruber, W. Wulfhekel, B. J. Hattink, and B. Poelsema, Phys. Rev. B **57**, R6803 (1998).
[32]M. Li and E. I. Altman, Phys. Rev. B **66**, 115313 (2002).
[33]G. J. Xu, K. S. Nakayama, B. R. Trenhaile, C. M. Aldao, and J. H. Weaver, Phys. Rev. B **67**, 125321 (2003).
[34]J. Wang, M. Li, and E. I. Altman, Surf. Sci. **596**, 126 (2005).
[35]T. M. Galea, C. Ordas, H. J. W. Zandvliet, and B. Poelsema, Phys. Rev. B **62**, 7206 (2000).
[36]H. J. W. Zandvliet, Phys. Rep. **388**, 1 (2003).
[37]D. J. Chadi, Phys. Rev. **59**, 1691 (1987).
[38]J. Tersoff and R. M. Tromp, Phys. Rev. Lett. **70**, 2782 (1993).
[39]X. Zeng and H. E. Elsayed-Ali, Surf. Sci. **497**, 373 (2002).
[40]J. Wang, M. Li, and E. I. Altman, Phys. Rev. B **70**, 233312 (2004).
[41]A. van Houselt, M. Fischer, B. Poelsema, and H. J. W. Zandvliet, Phys. Rev. B **78**, 233410 (2008).
[42]R. van Gastel, N. C. Bartelt, P. J. Feibelman, F. Léonard, and G. L. Kellogg, Phys. Rev. B **70**, 245413 (2004).
[43]M. L. Anderson, N. C. Bartelt, P. J. Feibelman, B. S. Swartzentruber, and G. L. Kellogg, Phys. Rev. Lett. **98**, 096106 (2007).
[44]J. Wang, M. Li, and E. I. Altman, Surf. Sci. **560**, 12 (2004).
[45]C. Priester and M. Lannoo, Phys. Rev. Lett. **75**, 93 (1995).
[46]F. Liu, A. H. Li, and M. G. Lagally, Phys. Rev. Lett. **87**, 126103 (2001).
[47]Albert-László Barabási, Appl. Phys. Lett. **70**, 2565 (1997).